Korean J. Chem. Eng., 35(9), 1807-1814 (2018)
DOI: 10.1007/s11814-018-0097-6

pISSN: 0256-1115
eISSN: 1975-7220

Fe-doped $LaCoO_3$ perovskite catalyst for NO oxidation in the post-treatment of marine diesel engine's exhaust emissions

So Ra An*,, Kyoung Ho Song*,**, Kwan Young Lee**, Ki Tae Park*, Soon Kwan Jeong*, and Hak Joo Kim*,†**

*Greenhouse Gas Research Laboratory, Korea Institute of Energy Research, Daejeon 34129, Korea
**Department of Chemical and Biological Engineering, Korea University, Seoul 02841, Korea
(*Received 5 December 2017 • accepted 13 June 2018*)

Abstract−New post-treatment process for marine diesel engine exhaust emissions was proposed by combining NO oxidation and wet scrubbing technology for the simultaneous removal of SO_X, NO_X and PM. NO, insoluble in aqueous scrubbing absorbent, is preferentially oxidized to NO_2, which then turns fully soluble in it. Fe substituted $LaCo_{1-x}Fe_xO_3$ perovskite catalysts were developed for NO oxidation to NO_2. The catalysts were prepared by co-precipitation method and analyzed with XRD, XRF, BET, FT-IR, NO-TPD and XPS techniques. Crystal structure change from rhombohedral to orthorhombic was observed with the increased amount of Fe substituted in the B site of the perovskite by XRD analysis. From FT-IR and NO-TPD analysis, nitrate on perovskite species was found to be the active species for NO oxidation. Quantitative analysis was performed within the prepared catalysts. Catalytic activity was measured using a packed bed reactor operated at 150-400 °C, atmospheric pressure and with gas hourly space velocity (GHSV) of 20,000 h^{-1} using a simulated exhaust gas composed of NO 400 ppm, O_2 10% balanced with N_2. Formation of Fe^{4+} cation enhanced the redox property as well as the mobility of the lattice oxygen present in the perovskite catalysts, confirmed by XPS analysis. Reaction mechanism of NO oxidation on Fe substituted $LaCo_{1-x}Fe_xO_3$ was discussed based on Mars-van Krevelen mechanism.

Keywords: Marine Exhaust Gas, NO Oxidation, Diesel Oxidation Catalyst (DOC), Perovskite Catalyst, Oxygen Vacancy, Mono- & Bi-dentate NO Adsorption, Fourier Transform-infrared Spectroscopy (FT-IR)

INTRODUCTION

Usage of low grade fuel containing sulfur in diesel engines in the field of marine transportation has led to air pollution in the largest container ports. According to a recent report [1], Busan has been nominated as one of the world's ten most air polluted ports from the usage of dirty marine fuel oil. The exhaust emissions from marine diesel engines are generally composed of carbon mono & dioxide (CO_X), nitrogen oxides (NO_X), volatile organic compounds (VOCs), sulfur oxides (SO_X), black carbon (BC) and particulate matter (PM). In particular, NO_X and SO_X not only have a direct primary effect on the human body, but also produce fine dust, acid rain and smog as secondary pollutants, resulting in serious environmental changes [2].

The International Maritime Organization (IMO) has been authorized to regulate emission from ships in the marine transportation sector. The International Convention for the Prevention of Pollution from Ships (MARPOL) was legislated in 1973. Current maritime emission regulations set limits for SO_X and NO_X for health and environmental reasons, and for CO_2 to mitigate global warming [3]. IMO regulations on nitrogen oxides are under effect to achieve NO_X emissions reduction through Tiers III for ships newly built after the year 2016. Multiple technologies such as exhaust gas recirculation (EGR), selective catalytic reduction (SCR), wet flue gas desulfurization (WFGD) combined with diesel oxidation catalysts (DOC) can be applied to meet the Tier III limits [4,5]. While SO_X regulation of IMO is imposed based on the sulfur content in the fuel. Ships can meet the requirement by using low sulfur compliant fuel oil or by using approved equivalent methods such as exhaust gas cleaning systems before emissions are released into the atmosphere. Among the technologies for SO_X removal from diesel marine engines, wet flue gas desulfurization (WFGD) has been widely used and reported as the best available process. Development of compact, effective and economic marine diesel engine exhaust gas cleaning system is required to meet the new IMO regulations on NO_X, SO_X and PM. A novel post-treatment process is proposed using WFGD combined with NO oxidation for the simultaneous removal of SO_X, NO_X and PM in a single scrubber. The conversion of NO to NO_2 facilitates the absorption of NO_X in the scrubber due to high solubility of NO_2 in basic absorption solution. Thus, NO_X, SO_X and PM can be removed simultaneously in a single scrubber making the exhaust gas cleaning system compact.

Platinum-based catalysts have been widely used as NO oxidation [6] and are actually the only commercially available catalysts. Després et al. reported that Pt/SiO_2 (2.5 wt%) converted about 80% of NO oxidation to NO_2 at 300 °C [7]. However, the use of noble metal resulted in high cost, as well as the collapse of the pore structure and noble metal agglomeration deactivated the catalysts easily under highly oxidative conditions [8]. In recent years, perovskite catalyst instead of precious metal catalyst has been attracting attention due to its low cost, high activity and thermal stability in the oxidation

†To whom correspondence should be addressed.
E-mail: hakjukim@kier.re.kr

process [9]. Wen et al. studied the high activity of Ce-doped perovskite catalysts ($La_{1-x}Ce_xCoO_3$) for NO oxidation [10]. Kim et al. observed that Sr-doped perovskite ($La_{0.9}Sr_{0.1}CoO_3$) catalyst showed better NO oxidation activity than the Pt based catalyst [11]. Shen et al. found that $La_{0.9}Ca_{0.1}MnO_3$ perovskite exhibited higher activity for NO oxidation and could convert 82% of NO at 300 °C [12]. Yoon et al. studied $La_{0.8}Ag_{0.2}MnO_3$ with the best activity for NO oxidation among the $La_{1-x}Ag_xMnO_3$ catalysts [13]. However B site doped perovskite in NO oxidation has rarely been reported. Wang et al. reported active $LaMn_{0.9}Co_{0.1}O_3$ perovskite catalysts for NO oxidation [14], while Zhou et al. showed 82% NO conversion for $LaCo_{0.9}Cu_{0.1}O_3$ catalyst at 310 °C [15]. $LaCoO_3$ and $LaMnO_3$ generally exhibit higher activity [16], but are less stable at higher temperatures than thermally stable $LaFeO_3$ catalyst [17].

In this study, we prepared Fe substituted $LaCo_{1-x}Fe_xO_3$ catalysts, characterized and tested for NO Oxidation. Fe^{4+} species was found to be generated with the substitution of Fe in the perovskite structure, which led to the weakening of B-O bond. The weakened B-O bond was presumed to increase the lattice oxygen transfer to the adsorbed NO as bidentate and bridged nitrate species for the oxidation to NO_2. The generated oxygen vacancies were instantaneously filled with the gas phase oxygen from the feed. NO oxidation on Fe substituted $LaCo_{1-x}Fe_xO_3$ catalysts was fulfilled by the oxidation of NO adsorbed on perovskite catalyst with lattice oxygen via Mars-van Krevelen mechanism.

EXPERIMENTAL

1. Catalyst Preparation

Fe substituted $LaCo_{1-x}Fe_xO_3$ catalysts were prepared using $La(NO_3)_3 \cdot 6H_2O$, $Co(NO_3)_2 \cdot 6H_2O$, and $Fe(NO_3)_3 \cdot 9H_2O$ as precursors. Na_2CO_3 was used as a precipitation agent to synthesize the catalysts. All the above precursors were in powder form and purchased from Sigma Aldrich. The perovskites $LaCo_{1-x}Fe_xO_3$ (x=0.0, 0.2, 0.3, 0.4, 1.0) catalysts were prepared by conventional co-precipitation method. 50 ml of deionized water was poured into a five-neck 500 ml flask and the temperature was adjusted to 80 °C. Appropriate amount of La, Co, Fe nitrates was dissolved in 150 ml of deionized water. The precursor solution was dropwise added into the five-neck flask at the rate of 5 ml/min under vigorous stirring. The pH of the solution was adjusted to 7-7.5 using the 1 M solution of Na_2CO_3 aqueous solution. The precipitates were aged for 1 h at 80 °C and washed sufficiently with hot deionized water. The washed precipitates were dried at 110 °C overnight, and subsequently calcined at 700 °C for 5 h under ambient atmosphere. Thus, prepared catalyst was denoted as $LaCo_{1-x}Fe_xO_3$, x=0 for $LaCoO_3$ and x=1 for $LaFeO_3$.

2. Catalyst Characterizations

The Brunauer-Emmett-Teller (BET) surface area, pore volume and pore diameter of the prepared catalysts were measured by the nitrogen adsorption isothermals at −196 °C (ASAP 2020, Micromeritics instrument). The samples were thermally pretreated at 100 °C under vacuum for 2 h. The metal content of the prepared catalysts was determined by wavelength dispersive X-ray fluorescence (XRF) spectrometry. The XRF spectrometer used in the analysis was Primus II (Rigaku Co., Japan). X-ray diffraction (XRD) patterns were obtained from supports and the fresh calcined catalysts using Rigaku D/MAX 2500V diffractometer with Ni filtered CuKα radiation. The diffraction patterns were scanned in 2θ range from 20° to 90°. Fourier-transform infrared spectroscopy (FT-IR) spectra were recorded in transmission mode on a Thermo Nicolet iS50 FT-IR spectrometer supplied with a DTGS detector (thermal detector). The powder samples diluted with KBr powder (1/100 w/w) were pressed into thin pellets using a pressure of 200 atm (sample mass about 150 mg). The transmittance spectra were obtained by collecting 32 scans at 4 cm^{-1} resolution. In NO temperature-programmed desorption (NO-TPD) experiment, 0.1 g of the catalyst was pretreated in N_2 at 400 °C for 1 h followed by cooling to 50 °C. After purging with N_2 for 30 min, the gas flow was switched to 400 ppm NO with N_2 balance. After the adsorption was completed, pure N_2 was introduced. The desorption involved heating the samples at a rate of 5 °C/min from 50 °C to 500 °C with pure N_2. X-ray photoelectron spectroscopy (XPS) analysis was performed on an AXIS Ultra DLD (Kratos Inc.) using a monochromatic Al Kα X-ray source (1486.6 eV). The binding energies were corrected by the C1s peak of carbon at 284.8 eV.

3. Catalytic Activity Measurement

The reaction system used for the measurement of the catalyst activity was a continuous flow type fixed bed reactor, made of quartz tube with inner diameter of 7 mm and height of 250 mm. Quartz wool and beads were used to fix the catalyst layer. In addition, the temperature of the catalyst bed was controlled by a PID temperature controller using a K-type thermocouple mounted on the top of the bed. Precise flow control of reactants, nitric oxide, oxygen and nitrogen was attained with the aid of mass flow controller (Brooks) under atmospheric pressure. Diesel engine exhaust emission was simulated with a mixture of 400 ppm NO, 10% O_2 in N_2 balance. The activity of the catalysts was tested at 150-400 °C and GHSV 20,000 h^{-1}. The gas concentration of the effluent stream was measured in situ by a gas detector tube (Gastec NO & NO_2 (11S, 10), Gastec Co., Ltd., Tokyo). Conversion of nitrogen oxides (NO_X) and nitrogen balance were calculated using the following equations:

$$NO_X \text{ conversion } (\%) = \left(1 - \frac{\text{NO molar flow rate in the product stream}}{\text{NO molar flow rate in the feed stream}}\right) \times 100(\%)$$

$$\text{N balance } (\%) = \left(1 - \frac{[\text{NO} + \text{NO}_2] \text{ molar flow rate in the product stream}}{\text{NO molar flow rate in the feed stream}}\right) \times 100(\%)$$

N balance was maintained within (100±1) % during each reaction experiment.

RESULTS AND DISCUSSION

1. Structure of Catalysts

Cobalt and iron under the form of trivalent cations have ion radius, which allows their crystallization in a perovskite ABO_3 structure when combined with lanthanum in the A site [18]. $LaCoO_3$ and $LaFeO_3$ are reported to have different crystal structures in different space group. $LaCoO_3$ has rhombohedral crystal structure with main diffraction peaks divided into 2θ=33.04° (1 1 0) and 2θ=33.4° (1 0 4). $LaFeO_3$ is orthorhombic and has a main diffraction peak at 2θ=32.2° (1 2 1). The difference between the two struc-

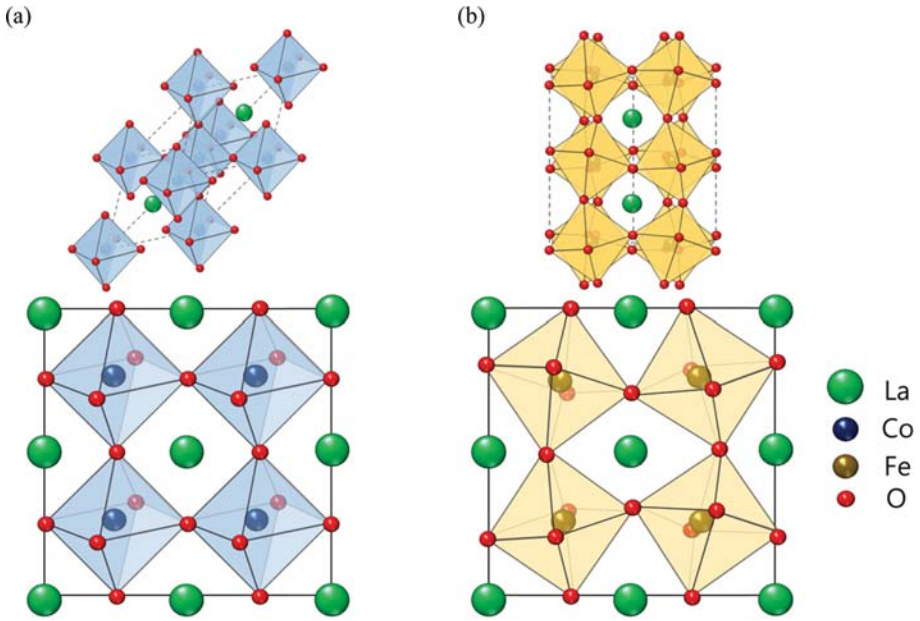

Fig. 1. (a) Rhombohedral structure of $LaCoO_3$, (b) Orthorhombic structure of $LaFeO_3$.

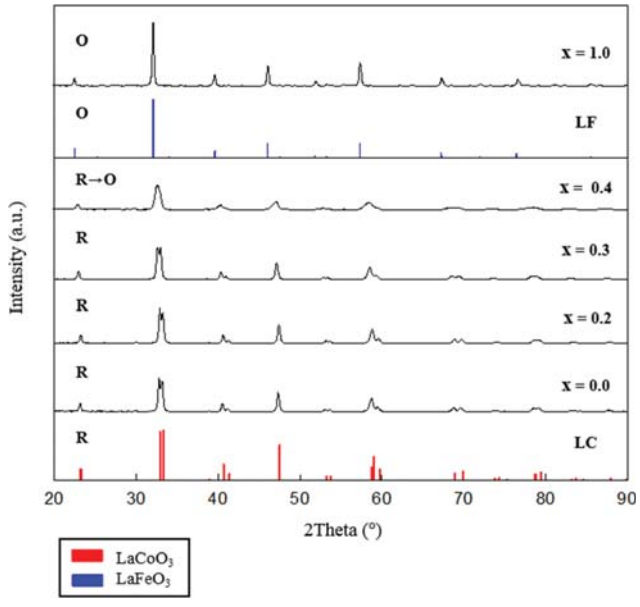

Fig. 2. XRD spectra of $LaCo_{1-x}Fe_xO_3$ (x=0.0, 0.2, 0.3, 0.4, 1.0) (R= Rhombohedral, O=Orthorhombic).

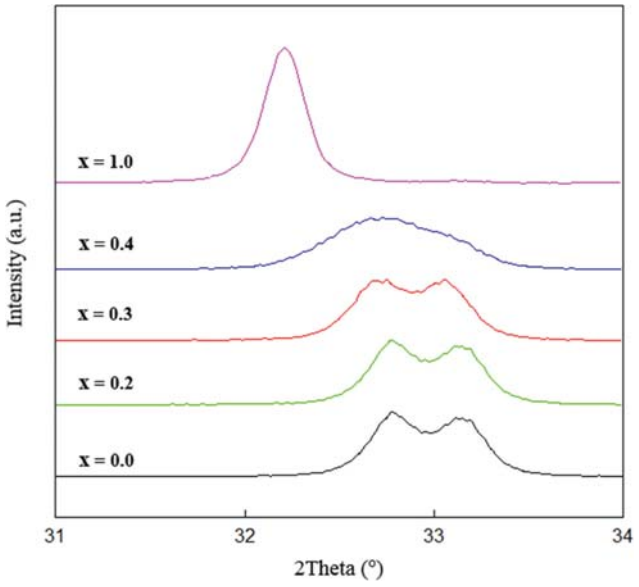

Fig. 3. Enlarged XRD patterns of $LaCo_{1-x}Fe_xO_3$ catalysts.

tures is that the distortion of the iron-coordinated octahedral arrangement is larger than that of cobalt as illustrated in Fig. 1.

The crystal structure of Fe substituted $LaCo_{1-x}Fe_xO_3$ was determined by XRD analysis. Fig. 2 shows the diffraction patterns of the $LaCo_{1-x}Fe_xO_3$ catalysts calcined at 700 °C. XRD patterns of reference rhombohedral $LaCoO_3$ (JCPDS-ICDD, 48-0123) and orthorhombic $LaFeO_3$ (JCPDS-ICDD, 37-1493) are shown in red and blue bars, respectively. The prepared $LaCoO_3$ and $LaFeO_3$ catalysts were found to have the rhombohedral and orthorhombic phases consistent with the patterns of the reference samples from JCPDS database. Enlarged XRD patterns of the $LaCo_{1-x}Fe_xO_3$ catalysts from 2θ angle 31° to 34° are presented in Fig. 3. As mentioned, $LaCoO_3$ (x=0) showed rhombohedral crystal structure with doublet peaks around 2θ angle of 33° (d=2.711 Å, 2.679 Å). As substituted iron content (x) increased, the doublet peaks tended to shift to lower angles. When the substituted iron content reached x=0.4, the doublet peaks were transformed into a broad single peak. This phenomenon was believed as the fact that with increased amount of substituted iron the crystal structure of rhombohedral was deformed and transformed into orthorhombic structure. It can finally be concluded that the maximum substituted iron content having rhombohedral crystal structure was around x=0.3. The shift of peaks was practically linear in relation to the Fe content, which was

Table 1. Metal composition and physical properties of the catalysts

Sample	Metal composition (at%)*			BET surface area (m^2/g)	Pore volume (cm^3/g)	Pore diameter (Å)
	La	Co	Fe			
$LaCoO_3$	50.3	49.7	-	10.0	0.021	83
$LaCo_{0.8}Fe_{0.2}O_3$	49.5	40.5	9.9	9.7	0.025	103
$LaCo_{0.7}Fe_{0.3}O_3$	49.7	35.7	14.6	8.6	0.017	78
$LaCo_{0.6}Fe_{0.4}O_3$	49.6	30.5	19.9	8.0	0.016	81
$LaFeO_3$	50.2	-	49.8	11.0	0.059	213

*Measured by XRF

thought to be due to the expansion of the unit cell. This expansion can be explained by the difference in ionic radius that can exist in the structure. The Co^{3+} and Fe^{3+} ion radius are reported to be 0.610 Å and 0.645 Å, respectively [19]. The ion radius of Co^{3+} and Fe^{3+} is very close but sufficient enough to cause expansion of the unit cell volume. The higher volume of the unit cell could be associated with decreased strength of the B-O bond.

2. Physical Properties of the Prepared Catalysts

ABO_3 perovskite catalysts are generally prepared with an equimolar ratio of A and B. The type of cation and its content for A site was fixed with La and to 50 at%, while for the B site cation Co was chosen as the main cation substituted with Fe ranging from 10 to 20 at%. The metal composition of the prepared catalysts measured by XRF spectrometer is summarized in Table 1. The compositions of the prepared catalysts were in close agreement with the nominal compositions.

The specific surface areas (SSA) of the catalysts measured by BET isotherms are given in Table 1. Since perovskites are highly crystallized materials obtained at high temperature, the prepared $LaCo_{1-x}Fe_xO_3$ catalysts showed poor specific surface area ranging from 7 to 11 m^2/g. As mentioned, with the substitution of Fe in $LaCoO_3$ the unit cell volume was expected to expand, which allowed denser crystallite structure. This phenomenon happened because the Fe^{3+} cation radius was larger than that of Co^{3+}. Thus, the Fe substituted $LaCo_{1-x}Fe_xO_3$ catalysts had an expanded and distorted crystal structure compared with that of the bare $LaCoO_3$. As a result, the SSA of the $LaCo_{1-x}Fe_xO_3$ catalysts decreased linearly with the content of the substituted Fe. On the other hand, $LaFeO_3$ had a completely different crystal structure with larger Fe^{3+} cation, which led to the formation of large pores with higher surface area. Merino et al. showed that the crystallization of the $LaCo_{1-x}Fe_xO_3$ structure started at 550 °C similar to $LaCoO_3$, and a significant decrease in SSA was observed when increasing the calcination temperature from 700 to 800 °C [20]. Therefore, the calcination temperature in this work was chosen as 700 °C based on their previous study.

3. Fourier Transform-infrared Spectroscopy (FT-IR)

To identify the intermediate chemical species of NO adsorbed on the surface of the catalysts, FT-IR analysis was performed with the prepared $LaCo_{1-x}Fe_xO_3$ catalysts. The results are shown in Fig. 4 and Table 2. Characteristic absorption bands of NO on perovskite material appeared between 1,000 and 1,800 cm^{-1}. The bands in this region were assigned to the adsorbed nitrate species. Three different kinds of nitrate were clearly observed: monodentate (1,273 cm^{-1}), bidentate (1,516-1,522 cm^{-1}), and the bridging nitrate (1,065 and 1,635 cm^{-1}). These nitrate species are commonly recognized as the key reaction intermediates for NO oxidation [21-25]. The structure and the band wavenumber of the adsorbed NO species on the Fe substituted $LaCo_{1-x}Fe_xO_3$ catalysts are summarized in Table 2. The main NO adsorption band appeared at 1,516-1,522 cm^{-1} on all the prepared catalysts as bidentate nitrate. Monodentate nitrate species were also observed at 1,273 cm^{-1} on Fe substituted $LaCo_{1-x}Fe_xO_3$ catalysts (x=0, 0.2, 0.3, 0.4), while the intensity of that band decreased sharply with $LaFeO_3$ (x=1.0) catalyst. Bridging nitrate species were also detected on all the prepared catalysts with low intensity, showing that bridging nitrate species were rather more unstable than the two other ones.

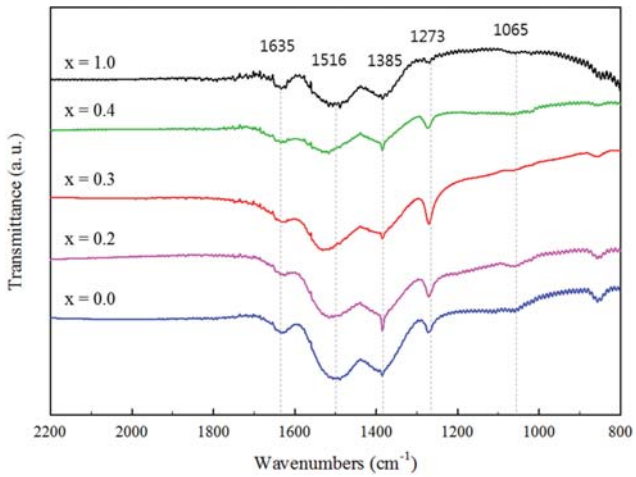

Fig. 4. FT-IR spectra of $LaCo_{1-x}Fe_xO_3$ catalysts.

Table 2. The species and structure of NO absorbed into the catalyst via the FT-IR

NO_X species	Structure	Wavenumber (cm^{-1})
Free nitrate ion, NO_3^-		1386
Monodentate nitrate	M-O-NO_2	1273
Bidentate nitrate	M-O_2NO	1516
Bridging nitrate	$(M-O)_2$=NO	1065, 1635

4. NO Temperature-programmed Desorption (NO-TPD)

NO-TPD analysis was performed for the quantitative and qualitative analysis of NO adsorption/desorption behavior on $LaCo_{1-x}Fe_xO_3$ catalysts, and the results are illustrated in Fig. 5. All profiles can be

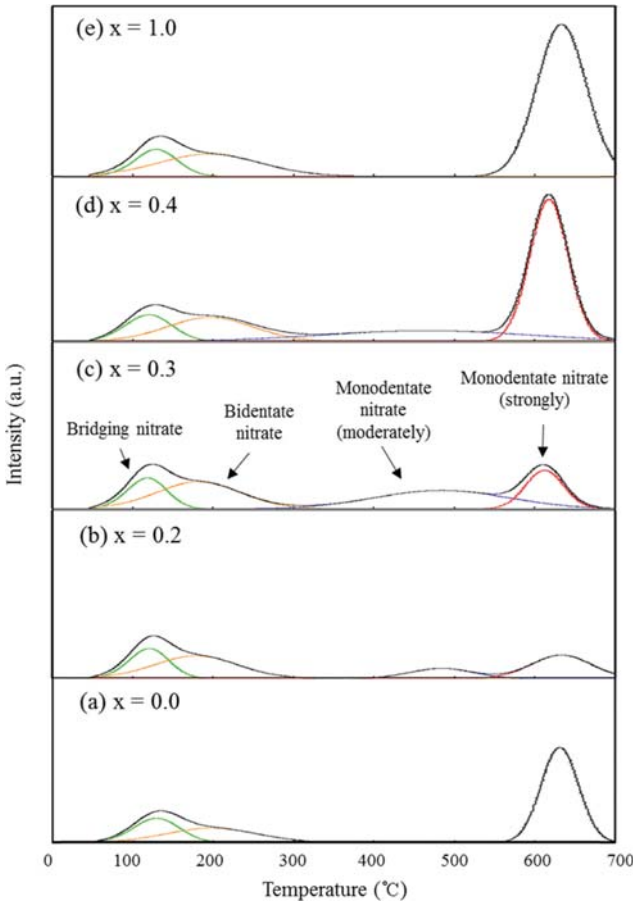

Fig. 5. NO-TPD profiles of the $LaCo_{1-x}Fe_xO_3$ catalysts.

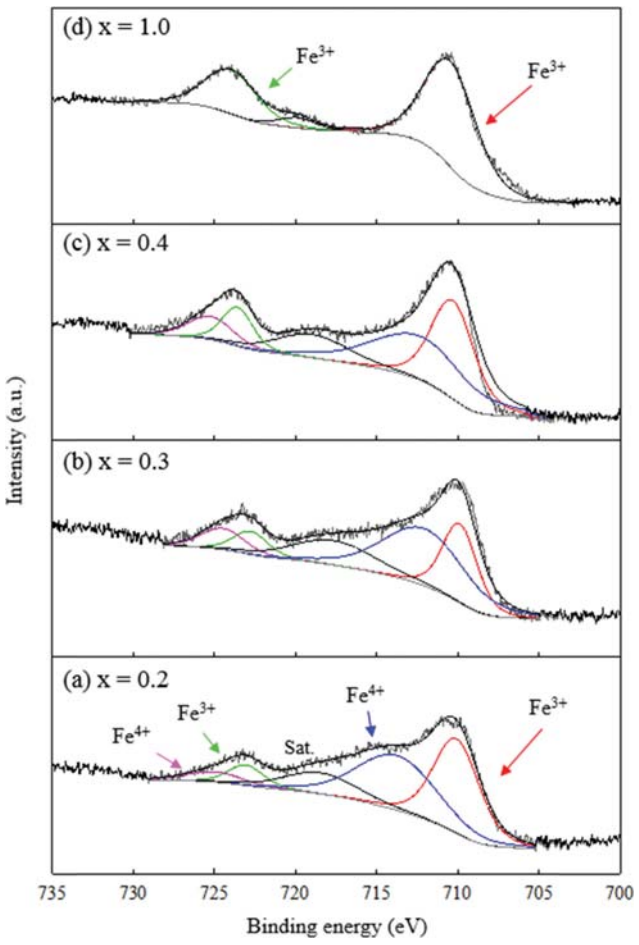

Fig. 6. Fe 2p spectra of the $LaCo_{1-x}Fe_xO_3$ catalysts.

deconvoluted into three or four Gaussian peaks. Results of qualitative analysis from the deconvolution of the NO-TPD profiles are summarized in Table 3, assuming four different adsorbed NO species. Three types of adsorbed NO were observed in common for all the prepared $LaCo_{1-x}Fe_xO_3$ catalysts. The most weakly adsorbed bridging nitrate NO desorbed at the temperature below 150 °C [26]. The desorption peaks around 200 °C were assigned to the NO adsorbed as bidentate nitrate species [27]. Monodentate nitrate species strongly adsorbed on the perovskite catalysts were desorbed at high temperature up to 600 °C [28]. For Fe substituted $LaCo_{1-x}Fe_xO_3$ catalysts (x=0.2, 0.3, 0.4), a broad satellite desorption peak was observed in the temperature range between 300 and 500 °C. This desorption peak was assigned to the monodentate nitrate species moderately bound to the B-O bond present in the Fe substituted $LaCo_{1-x}Fe_xO_3$ catalysts as discussed earlier. As presented in Table 3, the amount of the moderately bound monodentate nitrate species increased with the content of substituted Fe until the substitution ratio of x=0.3 then tended to decrease. In contrast, the amount of strongly bound monodentate nitrate species were found to be three- to five-times higher for $LaCoO_3$ and $LaFeO_3$ catalyst compared with those of the Fe substituted $LaCo_{1-x}Fe_xO_3$ catalysts. Discriminatively, $LaCo_{0.6}Fe_{0.4}O_3$ (x=0.4) catalyst had both large amount of moderately and strongly bound monodentate nitrate species, as much as 24.0 and 60.9 μmol/g, respectively. Reasonable correlation between the absorption band at 1,273 cm^{-1} in the FT-IR anal-

Table 3. Amounts of NO desorbed from $LaCo_{1-x}Fe_xO_3$ catalysts during NO-TPD

Sample	Bridging nitrate (μmol/g) (100 °C)	Bidentate nitrate (μmol/g) (200 °C)	Monodentate nitrate (moderate) (μmol/g) (300-500 °C)	Monodentate nitrate (strong) (μmol/g) (600 °C)
$LaCoO_3$	12.5	14.9	-	40.2
$LaCo_{0.8}Fe_{0.2}O_3$	12.8	20.9	6.9	15.4
$LaCo_{0.7}Fe_{0.3}O_3$	13.1	25.4	27.5	16.5
$LaCo_{0.6}Fe_{0.4}O_3$	13.4	22.8	24.0	60.9
$LaFeO_3$	12.3	24.7	-	82.6

ysis and mid-temperature (300-500 °C) desorption peak in NO-TPD can be made that with the substitution of Fe in $LaCoO_3$ catalyst, moderately adsorbed NO as monodentate nitrate species on perovskite was definitely generated, maximum in quantity with $LaCo_{0.7}Fe_{0.3}O_3$ catalyst.

5. X-ray Photoelectron Spectroscopy (XPS)

For further understanding of the derivation of the moderately adsorbed monodentate nitrate species, the chemical state of the surface elements was analyzed by XPS. No definite chemical shifts were observed within the La (3d5/2) at 834.0 eV and Co (2p) at 779.6 eV. As illustrated in Fig. 6, Fe^{3+} cation was the only Fe cation present in the ABO_3 type perovskite $LaFeO_3$ catalyst. In contrast, with the Fe substituted $LaCoO_3$ catalysts, both Fe^{3+} and Fe^{4+} cations were observed at the surface layers of the catalysts. The oxidation of Fe^{3+} to Fe^{4+} cation would generate the redox-coupled ion pair responsible for controlling the electronic mobility of the perovskite catalysts [29]. The Fe^{3+}-Fe^{4+} couple could play an important role on the catalytic behavior. Quantitative XPS analysis results are summarized in Table 4.

Table 4. Surface atomic ratios of $LaCo_{1-x}Fe_xO_3$ catalysts

Sample	Surface iron species (at%)		Surface oxygen species (at%)		
	Fe^{3+}	Fe^{4+}	O_{wat}	O_{ads}	O_{lat}
$LaCoO_3$	-	-	3.1	69.4	27.5
$LaCo_{0.8}Fe_{0.2}O_3$	50.6	49.4	14.7	49.9	35.4
$LaCo_{0.7}Fe_{0.3}O_3$	39.9	60.1	13.9	45.0	41.1
$LaCo_{0.6}Fe_{0.4}O_3$	51.0	49.0	4.1	55.8	40.1
$LaFeO_3$	100	-	5.1	55.6	39.3

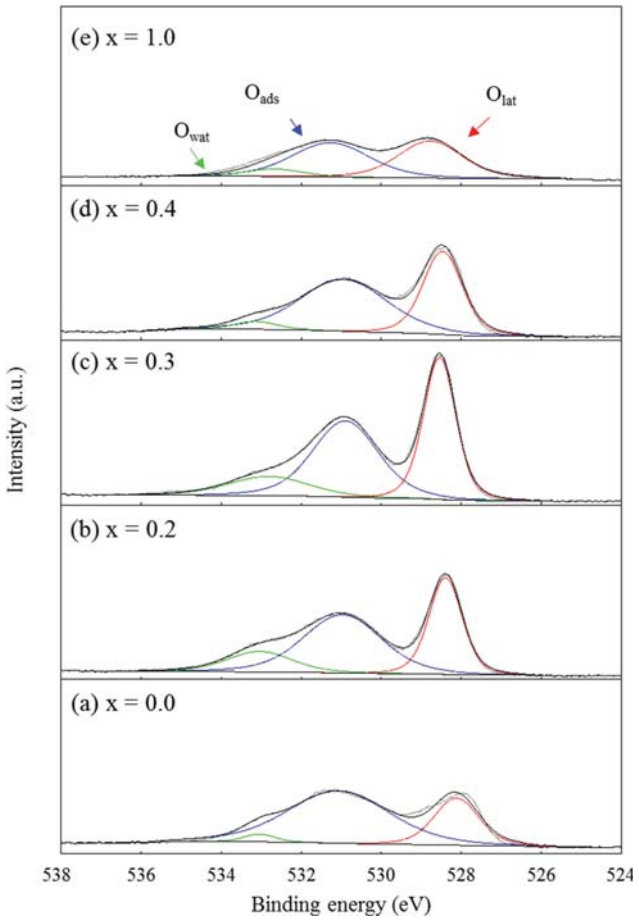

Fig. 7. O 1s spectra of the $LaCo_{1-x}Fe_xO_3$ catalysts.

The O 1s XPS spectra of $LaCo_{1-x}Fe_xO_3$ catalysts are shown in Fig. 7. It was found that there were three chemical states of oxygen. The peak with a low binding energy (528.1-528.8 eV) was attributed to the surface lattice oxygen (O_{lat}), the other one with a middle binding energy (530.9-531.3 eV) to the adsorbed oxygen species (O_{ads}), which are mainly stored on the surface in the form of carbonate, hydroxyl species and weakly bound oxygen. The last one with a high binding energy (532.7-533.1 eV) was assigned to the adsorbed molecular water (O_{wat}) [30]. As presented in Table 4, the amount of O_{lat} was found to increase with respect to the presence of Fe^{4+}. Among the prepared catalysts, $LaCo_{0.7}Fe_{0.3}O_3$ had the largest amount of O_{lat} as much as 41.1 at%.

6. Catalytic Activity

The NO oxidation performance of $LaCo_{1-x}Fe_xO_3$ (x=0.0, 0.2, 0.3, 0.4, 1.0) catalysts is presented in Fig. 8. The catalytic activity change of ABO_3 type perovskite $LaCoO_3$ was observed by replacing a part of B site cobalt with iron. The NO conversion of all $LaCo_{1-x}Fe_xO_3$ catalysts was about 25% at 150 °C and increased gradually to reach maximum activity at 250 °C near the equilibrium conversion. The temperature of the gas emission of marine diesel engines is typically from 190 to 240 °C. The NO conversion at the temperature window ranging from 190 to 240 °C is a matter of concern. In that temperature range, Fe substituted (x=0.2, 0.3, 0.4) $LaCo_{1-x}Fe_xO_3$ catalysts showed higher activity than $LaCoO_3$ and $LaFeO_3$ catalysts. Especially, $LaCo_{0.7}Fe_{0.3}O_3$ catalyst reached 91% NO conversion at 225 °C, which could meet the requirement needed to fulfill the Tier III regulation [31,32].

Integrating related analysis results, we finally concluded that Fe substituted $LaCo_{1-x}Fe_xO_3$ catalyst retained its rhombohedral crystal structure until the substitution ratio of x=0.3, but with expansion and distortion. The substitution of Fe in $LaCoO_3$ led to the

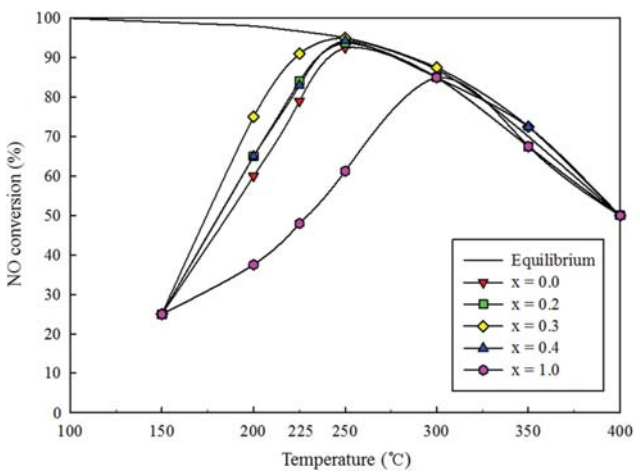

Fig. 8. NO concentration of $LaCo_{1-x}Fe_xO_3$ (x=0.0, 0.2, 0.3, 0.4, 1.0); (GHSV=20,000 hr^{-1}, NO 400 ppm, O_2 10% balanced N_2).

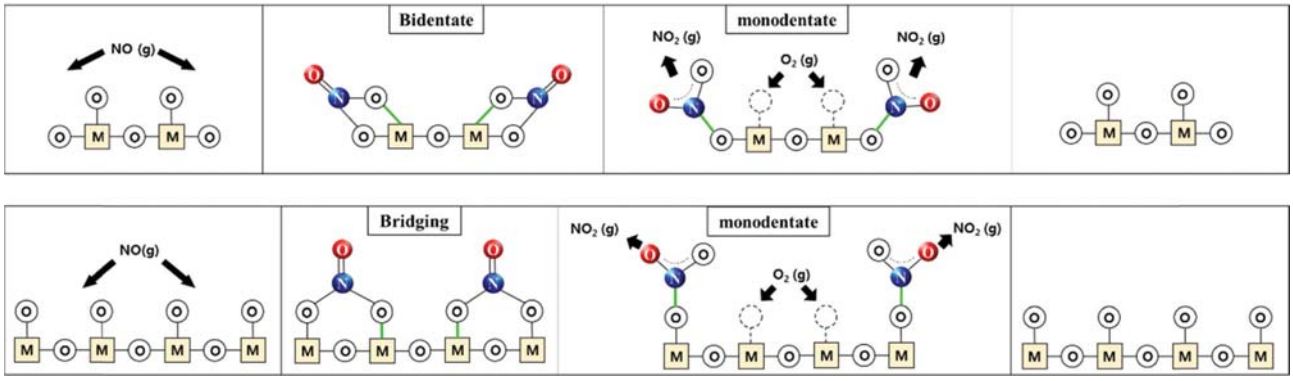

Fig. 9. The sequence of elementary steps for NO oxidation on $LaCo_{1-x}Fe_xO_3$ surface based on Mars-van Krevelen mechanism.

transformation of Fe^{4+} cation from Fe^{3+} present in pure $LaFeO_3$. Charge compensation via Fe^{4+} formation brought to an increase of lattice oxygen on the catalyst surface layers. Furthermore, the substitution of Fe in $LaCoO_3$ decreased the strength of the B-O bond. The lattice oxygen bound to Fe^{4+} cation might be easily transferred to the adsorbed NO as bidentate and bridging nitrates to form monodentate nitrate. The bridging nitrate could be generated when NO is adsorbed to dual lattice oxygens bound to different metals while bidentate nitrate to oxygens bound to a single metal. The cleavage of the B-O bond in the adsorbed monodentate nitrate leads to the formation of NO_2, which is reported as the rate determining step for NO oxidation to NO_2 [25].

7. Proposed Reaction Mechanism

To the best of our knowledge, a detailed reaction mechanism on NO oxidation over $LaCo_{1-x}Fe_xO_3$ perovskite catalyst has not been discussed in the literature. The four step reactions for NO oxidation are illustrated in Fig. 9. NO is first adsorbed as monodentate, bidentate and bridging nitrates. The formation of Fe^{4+} cation produced active sites with weakened strength of the B-O bond. Strongly adsorbed monodentate species might be formed with the adsorption of NO to the primitive strong B-O bond abundantly present in $LaCoO_3$ and $LaFeO_3$. Weakened B-O bond cleavages on bidentate and bridging nitrates enhanced the formation of moderately adsorbed monodentate species, which was further converted to NO_2. The oxygen vacancies were instantaneously filled with gaseous oxygen.

As mentioned previously, the substitution of Fe in $LaCoO_3$ increased the unit cell volume and distorted the crystal structure, which decreased the strength of B-O bond. Due to the complete rhombohedral and orthorhombic crystal structure for $LaCoO_3$ and $LaFeO_3$ perovskites, lattice oxygen mobility was affordable only at high temperatures. While for the Fe substituted $LaCoO_3$ catalysts, weakened B-O bond enhanced the mobility of the lattice oxygen for NO oxidation. The change of the micro-scale crystal structure might develop the formation of Fe^{4+} cation, which enhanced the redox property as well as the mobility of the lattice oxygen by the generation of moderately bound monodentate nitrate species.

CONCLUSIONS

Fe substituted in the B site of ABO_3 type $LaCoO_3$ perovskite catalyst was prepared by co-precipitation method for the NO oxidation. From XRD analysis, $LaCo_{0.7}Fe_{0.3}O_3$ catalyst retained the rhombohedral crystal structure with expanded unit cell, giving rise to the formation of lattice oxygen with weakened B-O bond. Substitution of Fe increased NO adsorption as moderately bound monodentate nitrate species confirmed by FT-IR and NO-TPD analysis. According to the XPS analysis, formation of Fe^{4+} cation changed the redox ion couple, enhancing the mobility of lattice oxygen to the surface layers of the Fe substituted perovskite catalyst. As Fe content was increased, charge compensation via Fe^{4+} formation was intensified. The optimum Fe substitution content was 15 at% (x=0.3), which showed 91% NO conversion at 225 °C meeting the Tier III regulations. Above 250 °C, most of the catalysts reached the equilibrium NO conversion. Reaction mechanism of NO oxidation on Fe substituted $LaCoO_3$ was proposed using Mars van Krevelen mechanism. NO was first adsorbed as bidentate and bridging nitrates, bound to the weakened B-O bond. The cleavage of that weakened B-O bond from the bidentate and bridging nitrates generated monodentate nitrate species, which was further desorbed as gas phase NO_2. The oxygen vacancies were instantaneously filled with gaseous oxygen. Fe substitution on $LaCoO_3$ catalyst increased the formation of Fe^{4+} cation, which enhanced the redox property as well as the mobility of the lattice oxygen by the generation of moderately bound monodentate nitrate species. The developed Fe substituted $LaCoO_3$ catalyst could be used for the post-treatment of marine diesel engines exhaust gas constituted of DOC and wet scrubbing for the simultaneous removal of NO_X, SO_X and PM.

ACKNOWLEDGEMENTS

This work was financially supported by the Grant-in-aid from the Ministry of Science and ICT, the Ministry of Environment and Korea Institute of Energy Research (Project B8-2431 & B7-6711).

REFERENCES

1. Z. Wan, M. Zhu, S. Chen and D. Sperling, *Nature*, **530**, 275 (2016).
2. Ministry of Environment Republic of Korea, Environmental Statistics Yearbook in 2002. http://eng.me.go.kr/eng/web/main.do/, 2017 (Accessed 4 March 2017).
3. M. S. Eide, S. B. Dalsøren, Ø. Endresen, B. Samset, G. Myhre, J.

Fuglestved and T. Berntsen, *Atmos. Chem. Phys.*, **13**, 4183 (2013).
4. Dieselnet, International: IMO Marine Engine Regulations, http://www.dieselnet.com/standards/inter/imo.php/2017 (Accessed 8 May 2017).
5. J. Wahlström, N. Karvosenoja and P. Porvari, Ship Emissions And Technical Emission Reduction Potential in the Northern Baltic Sea, *Finnish Environment Institute*, Helsinki (2006).
6. N. Kruse, A. Frennet and J. M. Bastin, *Catalysis and Automotive Pollution Control IV*, **116**, 199 (1998).
7. J. Despres, M. Elsener, M. Koebel, O. Kröcher, B. Schnyder and A. Wokaun, *Appl. Catal., B: Enviorn.*, **50**, 73 (2004).
8. D. M. Fernandes, C. F. Scofield, A. A. Neto, M. J. B. Cardoso and F. M. Z. Zotin, *Chem. Eng. J.*, **160**, 85 (2010).
9. S. Ponce, M. A. Pena and J. L. G. Fierro, *Appl. Catal., B: Enviorn.*, **24**, 193 (2000).
10. Y. Wen, C. Zhang, H. He, Y. Yu and Y. Teraoka, *Catal. Today*, **126**, 400 (2007).
11. C. H. Kim, G. Qi, K. Dahlberg and W. Li, *Science*, **327**, 1624 (2010).
12. S. Meiqing, Z. Zhen, C. Jiahao, S. Yugeng, W. Jun and W. Xinquan, *J. Rare Earths*, **31**, 119 (2013).
13. E. Lim, Y. J. Kim, J. H. Kim, T. Ryu, S. Lee, B. K. Cho and S. Yoo, *J. Catal.*, **319**, 182 (2014).
14. J. Wang, Y. Su, X. Wang, J. Chen, Z. Zhao and M. Shen, *Catal. Commun.*, **25**, 106 (2012).
15. C. Zhou, X. Liu, C. Wu, Y. Wen, Y. Xue, R. Chen and W. G. Wang, *Phys. Chem. Chem. Phys.*, **16**, 5106 (2014).
16. H. Najjar, J. F. Lamonier, O. Mentré, J. M. Giraudon and H. Batis, *Appl. Catal., B: Enviorn.*, **106**, 149 (2011).
17. H. Arai, T. Yamada, K. Eguchi and T. Seiyama, *Appl. Catal.*, **26**, 265 (1986).
18. L. Bedel, A. C. Roger, C. Estournes and A. Kiennemann, *Catal. Today*, **85**, 207 (2003).
19. R. D. Shannon, *Acta Crystallogr. A*, **32**, 751 (1976).
20. S. Lobos, M. Ganne and L. Bohan, *Simposio Iberoameriano de Catálisis*, II, 1267 (1998).
21. K. Hadjiivanov, *Catal. Lett.*, **68**, 157 (2000).
22. N. Tang, Y. Liu, H. Q. Wang and Z. B. Wu, *J. Phys. Chem. C*, **115**, 8214 (2011).
23. C. Sedlmair, K. Seshan, A. Jentys and J. A. Lercher, *J. Catal.*, **214**, 308 (2003).
24. J. Baltrusaitis, J. Schuttlefield, J. H. Jensen and V. H. Grassian, *Phys. Chem. Chem. Phys.*, **9**, 4970 (2007).
25. S. Thampy, Y. Zheng, S. Dillon, C. Liu, Y. Jangjou, Y.-J. Lee, W. S. Epling, K. Xiong, Y. J. Chabal, K. Cho and J. W. P. Hsu, *Catal. Today*, **310**, 195 (2018).
26. M. Machida, M. Uto, D. Kurogi and T. Kijima, *Chem. Mater.*, **12**, 3158 (2000).
27. S. J. Huang, A. B. Walters and M. A. Vannice, *J. Catal.*, **192**, 29 (2000).
28. J. Luo, F. Gao, D. H. Kim and C. H. Peden, *Catal. Today*, **231**, 164 (2014).
29. N. A. Merino, B. P. Barbero, P. Ruiz and L. E. Cadús, *J. Catal.*, **240**, 245 (2006).
30. R. G. de la Cruz, H. Falcon, M. A. Pena and J. L. G. Fierro, *Appl. Catal., B: Environ.*, **33**, 45 (2001).
31. W. A. Majewski, J. L. Ambs and K. Bickel, *SAE Technical Paper* 950374 (1995).
32. P. J. Schmitz, R. J. Kudla, A. R. Drews, A. E. Chen, C. K. Lowe-Ma, R. W. McCabe and C. T. Goralski, *Appl. Catal., B: Environ.*, **67**, 246 (2006).